Analysis of mitosis and anti-mitotic drug responses in tumors by in vivo microscopy and single-cell pharmacodynamics

Published in final edited form as:
Cancer Res. 2011 July 1; 71(13): 4608–4616. doi:10.1158/0008-5472.CAN-11-0412.

Analysis of mitosis and anti-mitotic drug responses in tumors by in vivo microscopy and single-cell pharmacodynamics

J.D. Orth[1,*], **R.H. Kohler**[2], **F Foijer**[1,3], **P.K. Sorger**[1], **R. Weissleder**[1,2], and **T.J. Mitchison**[1]

[1] Dept. Systems Biology, Harvard Medical School, 200 Longwood Ave, Boston, MA 02115

[2] Center for Systems Biology, Massachusetts General Hospital, 185 Cambridge St, Boston, MA 02114

[3] Wellcome Trust Sanger Institute, Wellcome Trust Genome Campus, Hinxton, CB10 1SA, UK

Abstract

Cancer relies upon frequent or abnormal cell division but how the tumor microenvironment affects mitotic processes in vivo remains unclear, largely due to the technical challenges of optical access, spatial resolution, and motion. We developed high-resolution in vivo microscopy methods to visualize mitosis in a murine xenograft model of human cancer. Using these methods, we determined whether the single-cell response to the anti-mitotic drug paclitaxel was the same in tumors as in cell culture; observed the impact of paclitaxel (Ptx) on the tumor response as a whole; and evaluated the single-cell pharmacodynamics of paclitaxel (by in vivo pharmacodynamic microscopy [IPDM]). Mitotic initiation was generally less frequent in tumors than in cell culture, but subsequently it proceeded normally. Paclitaxel treatment caused spindle assembly defects and mitotic arrest, followed by slippage from mitotic arrest, multinucleation and apoptosis. Compared to cell culture, the peak mitotic index in tumors exposed to paclitaxel was lower and the tumor cells survived longer after mitotic arrest, becoming multinucleated rather than dying directly from mitotic arrest. Thus, the tumor microenvironment was much less pro-apoptotic than cell culture. The morphologies associated with mitotic arrest were dose- and time-dependent, thereby providing a semi-quantitative, single-cell measure of pharmacodynamics. Although many tumor cells did not progress through Ptx-induced mitotic arrest, tumor significantly regressed in the model. Our findings demonstrate that in vivo microscopy offers a useful tool to visualize mitosis during tumor progression, drug responses, and cell fate at the single cell level.

Keywords

pharmacodynamics; in vivo microscopy; therapeutics; mitosis

Introduction

The bulk of cancer cell biology has been conducted using in vitro systems, with cells cultured in artificial environments. To better understand the origin and progression of cancer and chemotherapeutic drug responses we need in vivo imaging data, ideally at the single-cell level. Whole body imaging methods including optical, magnetic resonance imaging (MRI), positron emission tomography (PET) and computed tomography (CT) scans report on the state of tissues and diseases, but generally lack the resolution required for single cell analysis (1). High-resolution images can be obtained from histology, but this requires

Corresponding author: James D. Orth, Dept. Systems Biology, WAB541, Harvard Medical School, Boston, MA 02115, phone: 617 432 3728, fax: 617 432, james_orth@hms.harvard.edu.

invasive biopsies, or sacrificing animals at each time-point, without providing real-time data. Live-cell imaging in culture has revealed dynamic aspects of cancer cell biology and drug responses of single cells, but how these data apply to the situation in vivo is largely unknown. Thus, a clear need exists for sub-cellular resolution intravital microscopy (IVM) to correlate the acute responses of cells to drugs with the ultimate fates of cells, tumors and tissues in animal models of human disease. In rodents, IVM typically involves a glass window set into the animal, or an exteriorized organ (2–5) to directly observe underlying tissues and tumors (6–9). In optically favorable organisms such as zebra fish, drosophila and nematodes, IVM can visualize dynamic processes at the single cell level (10–12). But, most applications of IVM in rodents follow cells or groups of cells at relatively low-resolution. The challenges facing sub-cellular IVM include physiological motion, low signal to noise ratios and slow image capture rates that limit directly studying rapid intracellular processes and transient events at a quality comparable to culture systems. Overcoming these limitations requires addressing issues including light penetration, phototoxicity, and especially motion caused by breathing, heartbeat and muscle movements. Here, we report optimized IVM that enables highly detailed, sub-cellular light microscopy to study formation of the mitotic spindle and chromosome dynamics before and after drug delivery in xenograft tumors (Fig. 1a–c). Using this in vivo pharmacodynamic microscopy (IPDM), we analyzed the response of Paclitaxel (Ptx), an important anti-cancer mitotic drug, whose biology remains poorly understood at the whole-tumor level.

Mitosis is central to tumor growth and aneuploidy due to mitotic errors contributes to both tumorigenesis and the progression of cancer toward more aggressive genotypes (13). Anti-mitotic drugs that perturb microtubule dynamics are part of the chemotherapy regime for treating many cancers, and experimental drugs against other mitotic spindle proteins are in clinical trials (14). Ptx binds to microtubules, interferes with polymerization dynamics, promotes mitotic arrest, and triggers apoptosis in cancer cells (15–18). Time-lapse microscopy in culture has revealed important aspects of Ptx response dynamics and significant intra-cellular variability (Fig. 1d) (19). At saturating Ptx (typically 100–300nM) cells rarely die without first entering mitotic arrest that can last 24h or longer depending on the cell line (19). Post-arrest, cells either initiate apoptosis or exit without dividing into an abnormal G1-like state with multiple small nuclei; this abnormal mitotic exit is termed mitotic slippage (Fig. 1d) (20). Once multinucleated most cells cannot recover normal nuclear morphology and remain arrested, die, or attempt another mitosis that is typically multipolar (e.g. tripolar, not bipolar). Which of these pathways a given cell follows is highly variable both within a cell line and between cell lines (19, 21).

Although the effects of Ptx on microtubules and mitosis are well understood in culture (22, 23), many questions remain as to how it promotes tumor regression in vivo, why patients with the same diagnosis respond differently, and how resistance arises (24). One basic question is whether Ptx kills only cells that have entered mitosis in tumors, as in culture – i.e. is Ptx solely an anti-mitotic drug in the tumor context? Pharmacokinetic (PK; drug concentration vs. time) and PD (drug action vs. time) data are essential for understanding tumor responses. In contrast to the extensive information on the PK of Ptx (18, 25–27), its PD is complicated and requires better understanding via a development of biomarkers, ideally at multiple sequential steps in the drug action pathway. Two natural biomarkers for Ptx are mitotic arrest and cell death. These have been used as a PD biomarkers in rodent cancer models and man through scoring histology sections or stained biopsies (16, 28–30); multinucleation has been largely ignored. A dynamic readout of these biomarkers would be more powerful, especially if it could be calibrated to measure the relative Ptx concentration experienced by a tumor cell as a function of dose and time. Effects of Ptx on the morphology and duration of mitosis are concentration-dependent in cell culture (31, 32), suggesting these measurements might provide semi-quantitative PD biomarkers in tumors.

At low concentrations in culture (≤5nM), mitosis is delayed and often exhibits errors in chromosome alignment and segregation; at moderate concentrations (5–20nM) mitotic delays are longer, and cells often exhibit spindle multipolarity and multipolar division; at high concentrations (>20nM) cells arrest for many hours and then die or slip. These concentration-dependent responses have not been studied in vivo.

The questions we sought to answer included: (i) can tumor cells be visualized at a high enough resolution to observe single-chromosome errors during mitosis, and to discriminate different morphological biomarkers of Ptx action? (ii) how do Ptx responses differ in culture and in tumors, and are all Ptx effects in tumors mediated via mitotic arrest? (iii) can we quantify PD for a small molecule drug using live, sub-cellular imaging? To address these questions, human tumor cell lines known to establish xenograft tumors in nude mice were engineered to stably express fluorescent protein fusions to histone-H2b (to visualize chromatin) and/or β1-tubulin (to visualize microtubules). These cell lines report on cell-cycle state (interphase or mitotic), spindle morphology, mitotic errors such as lagging chromosomes, mitotic arrest, passage through mitotic arrest and apoptosis. We used dorsal skin-fold chambers (DSCs), and developed multiple approaches for immobilization and stabilization. Figure 1a depicts the main features of the set-up. HT-1080 cells rapidly established vascularized tumors in DSCs (Fig. 1b). Imaging with a 2X objective revealed overall tumor morphology and blood vessels, while our standard imaging conditions revealed detailed morphology (Fig. 1b).

Materials and Methods

Mice

Mice were housed and handled according to Harvard Medical Area Institutional Animal Care and Use Committee (HMA IACUC) guidelines. Nu/Nu mice (Cox-7; Massachusetts General Hospital, Boston MA) were anesthetized for DSC implantation by intraperitoneal injection of a 1:10 mixture of ketamine (50mg/ml, Bioniche Pharma, Lake Forest, IL) and xylazine (100mg/ml, Vedco, Inc. St. Joseph, MO) or by isoflurane vaporization (Harvard Apparatus, Holliston, MA) at a flow rate of 2.0liters/min isoflurane:2.0liters/min oxygen. For cell injection, injection of Ptx, and microscopy, mice were anesthetized by 2.0liters/min isoflurane:2.0liters/min oxygen. For >1 hour imaging, the isoflurane flow rate was slowly reduced to 0.8–1.2 liters/min. Surgeries were performed under sterile conditions using a zoom stereo-microscope (Olympus SZ61).

Dorsal skinfold chamber implantation

Titanium DSCs (APJ Trading Co, Inc.,Ventura CA) were implanted into the dorsal skin fold of Nu/Nu mice as described (2, 3, 7, 33). The DSC stretches and sandwiches the two layers of skin on the back of the mouse. On one side, the skin is surgically removed and replaced by a 10mm diameter optical glass cover slip held in place with a c-clip. Spacers between the two halves of the DSC frame prevent excess compression of the tissue and vessels. The window allows free access imaging of the remaining layers of striated skin muscle, subcutaneous tissue, deep dermis and tumors.

Cell injection into DSC

Cells were harvested by trypsinization (0.25% trypsin-EDTA) and resuspended in growth medium. Mice were anesthetized and ~10^6 (50μl) cells were injected subcutaneously using a 0.5cc insulin syringe (28½G, BD Biosciences, Chicago IL). The needle was bent at 90 degrees to aid injection. Injections were performed under a stereo-microscope. After injection, sterile saline was added into the DSC and it was closed with a new cover slip. For orientation and to establish a baseline for tumor growth, the cell mass was imaged 1–2 days

after injection. Tumors were rejected if there were any gross tissue abnormalities. The procedures resulted in no mortality and >95% of DSCs were adequate for microscopy. To evaluate and refine IVM methods, HeLa and U2 OS cells (which did not establish tumors in DSCs) were injected, with or without Ptx or Kinesin-5 inhibitor (K5I) pre-treatment in culture, and imaged within 7 days.

Paclitaxel and Kinesin-5 inhibitor treatment

To allow neovascularization, HT-1080 xenografts were grown ≥8 days before Ptx. Mice were injected tail vein with a single bolus of 1.2, 3, 6 or 30mg/kg Ptx (injectable formulation, Novaplus, Bedford Laboratories, Bedford, OH) diluted 1:4 with saline. 30mg/kg Ptx was used as the high dose based on published data (29, 34, 35). Kinesin-5 inhibitor EMD534085 (36) was from Merck Serono and was used in culture at 500nM.

Microscopy

To reduce motion artifacts and permit high-resolution microscopy over extended periods a DSC holder was designed (Fig. 1a). The set-up consists of an aluminum holder attached to an aluminum platform. The platform and DSC-holder were kept at 38°C to reduce thermal-drift. The screws of the DSC fit into machined holes in the holder and the DSC frame was further immobilized using small plates and screws. A charged-air table reduced vibration external to the instrumentation. 200μl of saline was injected intraperitoneal every hour during imaging to maintain hydration. For vascular imaging, fluorescein isothiocyanate-dextran (mol. wt. 2,000,000, Sigma-Aldrich, MO) or Angiosense-680 (mol. wt. 250,000 Perkin Elmer, Waltham, MA) was injected tail vein. A customized Olympus FV1000 based on a BX61-WI confocal microscope was used. Olympus objectives were: 25X XPlan N (NA 1.05, water), 2X/340 XLFluor (NA 0.14, air), 20X UPlanFL (NA 0.50) and 60X LUMFL N (NA 1.10, water). EGFP, mRFP, TagRFP and Angiosense-680 were excited using a 488 nm Argon ion laser-line, 559 nm pumped solid-state laser, or 635 nm diode laser, respectively, in combination with a DM405/488/559/635 nm dichroic beam splitter. Emitted light was separated and collected with beam splitters SDM560 and SDM640 and band-pass filters BA505–540, BA575–620, and BA655–757. Control tumors were used to optimize imaging conditions resulting in no photobleaching or phototoxicity. Using a motorized x-y stage, 5 z-stack time-series with 10–20 optical sections (5μm per section), at 30sec–5min intervals were collected. Small drifts in focus were corrected in real time using the z-adjustment feature of FluoView 1000 software.

Results

Visualization of detailed mitotic morphology in vivo

We used HT-1080 cells in all experiments but confirmed general concepts using HeLa and U2 OS. HeLa expressing both H2b-mRFP and mEGFP-α–tubulin were used to convey chromosomes and the mitotic spindle simultaneously (Fig. 2). Progression through normal mitosis was readily observed (Fig. 2a–d, Supplemental movie 1). At higher magnification, kinetochore fibers and spindle poles were well resolved (Fig. 2e) showing that critical mitotic structures can be studied in vivo using the IVM methods developed here; HT-1080 cells expressing H2b-EGFP or β1-tubulin-TagRFP gave comparable images.

To test our ability to discriminate morphologies associated with drug-induced perturbations, HeLa cells in culture were pre-treated with two drugs that induce morphologically distinct mitotic arrests, injected into DSCs and imaged (Fig. 2f,g). Ptx treated mitotic cells exhibited distributed rosettes of microtubules and scattered chromosomes (Fig. 2f) while K5I (36) treated cells exhibited characteristic monopolar spindles (Fig. 2g). Our ability to robustly distinguish the two different mitotic arrest phenotypes shows that IVM has sufficient

resolution to discriminate between related but distinct mitotic defects. As a more stringent test of resolution, U2 OS cells expressing the centromeric protein, CENP-B fused to EGFP were imaged. In either interphase (not shown) or mitotic cells, single CENP-B spots (≤500nm in size) were routinely resolved, which is consistent with the calculated diffraction limited resolution of our standard optics (~250nm). From these initial data, normal and mitotic arrest structures appear identical in culture and in vivo and we conclude that our cell models and methods will permit the identification of different mitotic spindle structures, and the imaging of chromosomes, as condensed human chromosomes are typically several microns in length.

To evaluate tubulin imaging as a drug response marker in vivo, HT-1080 expressing β1-tubulin-TagRFP were used (Supplemental Fig. 1). Without Ptx, normal interphase and mitotic cells were observed. After 30mg/kg Ptx, mitotic arrest with microtubule rosettes was observed in a subset of cells, confirming drug delivery and drug action on these cells (Supplemental Fig. 1, c–e). While tubulin imaging allowed visualization of mitosis and confirmation of Ptx action, fluorescent histone-H2b imaging reports on more features of drug response including mitotic spindle structures, chromosome behavior, mitotic arrest and slippage, and cell death and was therefore used in all subsequent experiments.

High-dose Paclitaxel effects

Since multiple mitotic structures and chromosomes could be resolved in DSCs, we used IVM to assay PD (IPDM) in HT-1080 xenograft tumors. Tumors in Ptx-treated (single bolus of 30mg/kg Ptx), mice showed few remaining tumors cells at day 17 (Supplemental Fig. 2a–d), in contrast to the vigorous tumors in saline-injected mice (not shown), indicating our model is highly sensitive to Ptx. Time-lapse z-series were collected at multiple random locations to reveal details of mitosis before and after drug. Time-lapse imaging was limited to 4h to minimize stress on the animals. Pre-drug we observed many examples of normal mitosis, but almost no examples of apoptosis (Supplemental movie 2). The average duration of mitosis was 1h 6min ± 6min, which is remarkably comparable to these cells in culture, 1h 18min ± 13min. 19h post-Ptx, the mitotic index was noticeably increased, and cells that entered mitosis during the time-lapse remained arrested (Fig. 3a–e, Supplemental movie 3). Few cells died during mitotic arrest (not shown), and no cells divided. Arrested cells often slipped from mitotic arrest and became multinucleated (Fig. 3f–j). Multinucleated cells did not re-enter mitosis but did sometimes die (Fig. 3b–e, i, j, Supplemental movies 3, 4). The morphology of cell death, during mitosis or from a multinucleated state, resembled apoptosis with chromatin condensation into multiple foci. Apoptotic bodies initially increased after Ptx (not shown), but did not accumulate over time, presumably due to macrophage clearance. The two image sequences in Figure 3a–e and f–j are from the same tumor, illustrating how cell populations in the same tumor can be imaged repeatedly over time to capture the dynamics of drug response.

The Ptx response was quantified by measuring mitotic and multinucleated index as a function of time (Fig. 3k). Mitotic index increased from~1.0% pre-Ptx to a ~7% maximum at 24h and then declined, reproducibly falling below baseline and reaching zero at 168h (Fig. 3k). The multinucleated index increased and peaked later than the mitotic index, and reached higher levels (~17%) presumably because multinucleation is persistent, lasting days in some cases, while mitotic arrest is transient, lasting hours (Fig. 3k). To compare PD measures in vivo and in culture, we scored Ptx effects on HT-1080 cells in culture by continuous time-lapse imaging (21). The control mitotic index pre-Ptx was ~7% in culture (Figure 3l) and in saturating Ptx (100nM), mitotic arrest peaked at 24h, with~75% arrest. By 48h Ptx, >90% of cells had died (Supplemental Fig. 3a). In contrast to the situation in tumors, ~95% of mitosis-arrested cells in culture initiated apoptosis without slipping from mitosis, and only ~5% slipped into the multinucleated G1 state before dying (Supplemental

Fig. 3, Supplemental movie 5). Death directly from mitotic arrest is characteristic of apoptosis sensitive cells in culture (37).

Mitotic defects at low Ptx concentrations

To test if IPDM could resolve subtle mitotic defects, including chromosome missegregation and multipolar mitoses, and to explore the utility of morphology as a quantitative PD marker, we also examined lower Ptx doses. At 1.2mg/kg, most mitotic cells showed no morphological defects (n = 199). At 3mg/kg, mitotic cells appeared normal in single, static images. Time-lapse imaging, however, revealed frequent defects. Mitosis often required >2h to complete, significantly longer than in untreated tumors (~1h). Figure 4a–c, (Supplemental movie 6) shows a representative cell in which the metaphase spindle took abnormally long (>2h) to assemble and a chromosome/chromosome pair failed to align properly (Fig. 4d, arrow, inset). Several stretched, lagging chromosomes were also evident at anaphase (Fig. 4e–g, Supplemental movie 6). These defects in chromosome segregation indicate abnormalities in kinetochore attachment and are frequently observed in cultured cells at low Ptx concentrations (31, 32). These data clearly demonstrate that time-lapse IPDM can reveal time-dependent mitotic phenotypes that are missed in single, static images.

The mitotic phenotype at 3mg/kg was mitotic delay and lagging chromosomes, so we increased the dose to 6mg/kg to test if we could induce spindle multipolarity as observed in culture at medium concentrations. In mice exposed to 6mg/kg Ptx and imaged 2–4h after dosing, dividing cells entered anaphase frequently with lagging chromosomes, sometimes resulting in daughter cells with micronuclei (Fig. 5a, Supplemental movie 7). By 24h, the mitotic index was increased, and many mitotic cells were multipolar, with some cells dividing into three or more daughters (Fig. 5b, Supplemental movie 8). These data suggest the effective concentration of Ptx in tumor cells increased and remained high from 2 to 24h, consistent with previous PK data (27). There appeared to be considerable cell-to-cell variability in tumors at 6mg/kg, in contrast to the uniform mitotic arrest observed at 30mg/kg.

Mitotic morphology as a pharmacodynamic marker

We used IPDM to quantify mitotic morphology as a function of dose and time up to 24h to determine if phenotype could be used as an effective measure of the Ptx concentration (Fig. 6a). Normal mitosis decreased and mitotic abnormalities increased with dose and time. Interestingly, multinucleated cells and multipolar mitoses peaked at intermediate doses (6mg/kg) and times (6h), showing that these morphologies report on exposure of cells to non-saturating drug concentrations. For high dose Ptx, multipolar mitoses peak at 2h, indicating Ptx had not reached saturation, but it had by 6h, as all mitotic cells were then arrested (Fig. 6a). The PD of Ptx during the first 24h in saturating conditions was dramatically different in tumors than in culture (Supplemental figure 4). In culture, by 2h all mitotic cells showed the arrested phenotype, the mitotic index increased rapidly, there was little multinucleation and by 24h 70% of cells had died. In tumors there was a delay in mitotic arrest phenotype, the mitotic index increased but remained comparatively low, and there was little death by 24h. These data show that Ptx-PD is significantly different in these tumors than in culture and IPDM can be used to characterize the Ptx concentration experienced by individual cells in tumors over time.

Discussion

Using optimized microscopic and animal preparations, we show that normal mitosis and anti-mitotic drug responses can be visualized at sub-cellular (≤500nm) spatial resolution in vivo (Fig. 2). The data show the power of IPDM to reveal detailed aspects of mitosis,

mitotic abnormalities, and drug-PD in tumors. These methods should be equally applicable to any organ that can be imaged through a window chamber or exteriorized, and perhaps to internal organs/tumors using multiphoton microscopy. Further, the general methods can be tailored, using specific probes, to study many different pathways in disease and cell biology in vivo. Using IPDM, we gained new insights into Ptx-PD in a tumor model that are summarized in Figure 6B for the saturating 30mg/kg dose, where we compare the effects of continuous exposure to saturating Ptx on the same cells in culture. The lower peak of mitotic arrest in tumors is consistent with a slower proliferation rate, but because the peak mitotic arrest occurred at 24h in both cases, the cell cycle transit time for cells that commit to divide must be similar. The low peak mitotic arrest in HT-1080 tumors resembles the response seen in other mouse cancer models by histology of tumor sections, and in human breast cancers by histology of fine needle aspirates (16, 29, 38). Mitosis-arrested cells tended to slip in tumors, and to die directly from mitotic arrest in culture. Presumably this reflects enhanced pro-survival signaling in the tumor, which allows slippage to win the kinetic competition with apoptosis induction (19, 39).

Pharmacokinetic studies of Ptx in mice showed that upon bolus i.v. injection at 40mg/kg, plasma levels peaked within 5 minutes (27, 34) but remained detectable for ≥14 days (34). Ptx has also been reported to be detectable within minutes of injection in a subcutaneous lung xenograft and several tissues, reach its peak concentration by ~2h, and remain detectable in these tissues for ≥14 days (34). Our PD data for 30mg/kg agrees well with this PK data as we observed mitotic arrest, indicating effective Ptx reaching the tumors, by 2h (Fig. 6, images not shown). The published half-life of Ptx (based on concentration determined using tritylated-Ptx and HPLC) in mouse tissues and lung xenograft tumors after a 40mg/kg dose was reported as ~50–70h (34) and our PD data at 30mg/kg shows Ptx remained maximally effective at 72h as all mitotic cells at this time were arrested. Further, at 72h Ptx remains high in the tumors because if washed away mitotic cells would be either normal or multipolar – this was not observed. From 72–168h post-Ptx, we noted a dramatic decrease of mitotic cells (Fig. 3k) and did not trap any dividing cells with a second dose of 30mg/kg Ptx at 168h after the first dose (not shown). These observations suggest the remaining tumor cells are no longer proliferating despite the fact that they are mostly mononucleated, implying they have not divided in Ptx. Ptx either damaged the remaining cells in a manner that is not evident from H2bEGFP imaging, and/or the tumor microenvironment has changed so that it no longer supports proliferation. This change is long-lasting in that xenograft tumors showed significant regression by two weeks (Supplemental Fig. 2). Consistent with these ideas, Symmans et al found some human breast cancers showed only a modest increase in mitotic index and little cell death in the first 48h after Ptx, but that these tumors later converted to a “sustained apoptotic response” (16). Elucidating how a modest mitotic arrest results in minimal cell killing in some tumors but translates into a sustained response with significant tumor clearance in others could be useful for improving anti-mitotic therapy.

The dose- and time-dependent effects revealed by IPDM show its potential to report on single-cell biomarkers. Tumors are genetically and environmentally heterogeneous, and individual cancer cells can respond differently to drugs even in culture (19, 21, 40). Cell-to-cell and intra-tumor heterogeneity are likely in tumors. Thus, PD biomarkers with sub-cellular resolution may prove very valuable in understanding drug responses. Further, based on our results with low-dose Ptx, it should be possible to visualize and quantify chromosome segregation defects that contribute to cancer progression in a tumor context using IPDM. IPDM is unique in its ability to reveal a dynamic response to drugs at the single cell level and allows for the use of many different probes including fluorescent dyes, particles, and antibodies, and probes for specific activities including kinases and proteases (1, 12, 41). In this study, a chromatin marker allowed us to study normal and abnormal mitotic progression

in real time at the resolution of single chromosomes, to monitor single cells responding to drug and undergoing apoptosis, and to establish drug PD over dose and time. The features of IPDM create a powerful technique with a bright future.

Supplementary Material

Refer to Web version on PubMed Central for supplementary material.

Acknowledgments

Financial support: NIH CA139980 to T.J.M. NIH CA084179 to P.K.S. NIH CA86355 and CA092782 to R.W.

Jose-Luiz Figueiredo and Rostic Gorbatov for help with mice. Soyeon Park for editorial assistance. The Center for Systems Biology platform for in vivo microscopy and the Nikon Imaging Center at Harvard Medical School.

References

1. Weissleder R, Pittet MJ. Imaging in the era of molecular oncology. Nature. 2008; 452(7187):580–9. [PubMed: 18385732]
2. Falkvoll KH, Rofstad EK, Brustad T, Marton P. A transparent chamber for the dorsal skin fold of athymic mice. Exp Cell Biol. 1984; 52(4):260–8. [PubMed: 6734890]
3. Lehr HA, Leunig M, Menger MD, Nolte D, Messmer K. Dorsal skinfold chamber technique for intravital microscopy in nude mice. Am J Pathol. 1993; 143(4):1055–62. [PubMed: 7692730]
4. Brown DL, Meagher PJ, Knight KR, et al. Survival and function of transplanted islet cells on an in vivo, vascularized tissue engineering platform in the rat: A pilot study. Cell Transplant. 2006; 15(4): 319–24. [PubMed: 16898225]
5. Fiorina P, Jurewicz M, Tanaka K, Behazin N, Augello A, Vergani A, et al. Characterization of donor dendritic cells and enhancement of dendritic cell efflux with CC-chemokine ligand 21: a novel strategy to prolong islet allograft survival. Diabetes. 2007; 56(4):912–20. [PubMed: 17287465]
6. Kedrin D, Gligorijevic B, Wyckoff J, Verkhusha VV, Condeelis J, Segall JE, et al. Intravital imaging of metastatic behavior through a mammary imaging window. Nat Methods. 2008; 5(12): 1019–21. [PubMed: 18997781]
7. Makale M. Intravital imaging and cell invasion. Methods Enzymol. 2007; 426:375–401. [PubMed: 17697892]
8. Wyckoff JB, Wang Y, Lin EY, Li JF, Goswami S, Stanley ER, et al. Direct visualization of macrophage-assisted tumor cell intravasation in mammary tumors. Cancer Res. 2007; 67(6):2649–56. [PubMed: 17363585]
9. Brown E, Munn LL, Fukumura D, Jain RK. In vivo imaging of tumors. Cold Spring Harb Protoc. 2010; 2010 pdb prot5452.
10. Gualda EJ, Filippidis G, Mari M, Voglis G, Vlachos M, Fotakis C, et al. In vivo imaging of neurodegeneration in Caenorhabditis elegans by third harmonic generation microscopy. J Microsc. 2008; 232(2):270–5. [PubMed: 19017226]
11. Yaniv K, Isogai S, Castranova D, Dye L, Hitomi J, Weinstein BM. Live imaging of lymphatic development in the zebrafish. Nat Med. 2006; 12(6):711–6. [PubMed: 16732279]
12. Weigert R, Sramkova M, Parente L, Amornphimoltham P, Masedunskas A. Intravital microscopy: a novel tool to study cell biology in living animals. Histochem Cell Biol. 2010; 133(5):481–91. [PubMed: 20372919]
13. Sen S. Aneuploidy and cancer. Curr Opin Oncol. 2000; 12(1):82–8. [PubMed: 10687734]
14. Jackson JR, Patrick DR, Dar MM, Huang PS. Targeted anti-mitotic therapies: can we improve on tubulin agents? Nat Rev Cancer. 2007; 7(2):107–17. [PubMed: 17251917]
15. Woods CM, Zhu J, McQueney PA, Bollag D, Lazarides E. Taxol-induced mitotic block triggers rapid onset of a p53-independent apoptotic pathway. Mol Med. 1995; 1(5):506–26. [PubMed: 8529117]

16. Symmans WF, Volm MD, Shapiro RL, Perkins AB, Kim AY, Demaria S, et al. Paclitaxel-induced apoptosis and mitotic arrest assessed by serial fine-needle aspiration: implications for early prediction of breast cancer response to neoadjuvant treatment. Clin Cancer Res. 2000; 6(12):4610–7. [PubMed: 11156210]
17. Sugimura M, Sagae S, Ishioka S, Nishioka Y, Tsukada K, Kudo R. Mechanisms of paclitaxel-induced apoptosis in an ovarian cancer cell line and its paclitaxel-resistant clone. Oncology. 2004; 66(1):53–61. [PubMed: 15031599]
18. Soma D, Kitayama J, Ishigami H, Kaisaki S, Nagawa H. Different tissue distribution of paclitaxel with intravenous and intraperitoneal administration. J Surg Res. 2009; 155(1):142–6. [PubMed: 19328496]
19. Gascoigne KE, Taylor SS. Cancer cells display profound intra- and interline variation following prolonged exposure to antimitotic drugs. Cancer Cell. 2008; 14(2):111–22. [PubMed: 18656424]
20. Brito DA, Rieder CL. Mitotic checkpoint slippage in humans occurs via cyclin B destruction in the presence of an active checkpoint. Curr Biol. 2006; 16(12):1194–200. [PubMed: 16782009]
21. Orth JD, Tang Y, Shi J, Loy CT, Amendt C, Wilm C, et al. Quantitative live imaging of cancer and normal cells treated with Kinesin-5 inhibitors indicates significant differences in phenotypic responses and cell fate. Mol Cancer Ther. 2008; 7(11):3480–9. [PubMed: 18974392]
22. Schiff PB, Horwitz SB. Taxol stabilizes microtubules in mouse fibroblast cells. Proc Natl Acad Sci U S A. 1980; 77(3):1561–5. [PubMed: 6103535]
23. Hadfield JA, Ducki S, Hirst N, McGown AT. Tubulin and microtubules as targets for anticancer drugs. Prog Cell Cycle Res. 2003; 5:309–25. [PubMed: 14593726]
24. Orr GA, Verdier-Pinard P, McDaid H, Horwitz SB. Mechanisms of Taxol resistance related to microtubules. Oncogene. 2003; 22(47):7280–95. [PubMed: 14576838]
25. Ishigami H, Kitayama J, Otani K, Kamei T, Soma D, Miyato H, et al. Phase I pharmacokinetic study of weekly intravenous and intraperitoneal paclitaxel combined with S-1 for advanced gastric cancer. Oncology. 2009; 76(5):311–4. [PubMed: 19299904]
26. Eiseman JL, Eddington ND, Leslie J, MacAuley C, Sentz DL, Zuhowski M, et al. Plasma pharmacokinetics and tissue distribution of paclitaxel in CD2F1 mice. Cancer Chemother Pharmacol. 1994; 34(6):465–71. [PubMed: 7923556]
27. Dhanikula AB, Singh DR, Panchagnula R. In vivo pharmacokinetic and tissue distribution studies in mice of alternative formulations for local and systemic delivery of Paclitaxel: gel, film, prodrug, liposomes and micelles. Curr Drug Deliv. 2005; 2(1):35–44. [PubMed: 16305406]
28. Milross CG, Mason KA, Hunter NR, Chung WK, Peters LJ, Milas L. Relationship of mitotic arrest and apoptosis to antitumor effect of paclitaxel. J Natl Cancer Inst. 1996; 88(18):1308–14. [PubMed: 8797771]
29. Milas L, Hunter NR, Kurdoglu B, Mason KA, Meyn RE, Stephens LC, et al. Kinetics of mitotic arrest and apoptosis in murine mammary and ovarian tumors treated with taxol. Cancer Chemother Pharmacol. 1995; 35(4):297–303. [PubMed: 7828272]
30. Chakravarthy A, Nicholson B, Kelley M, Beauchamp D, Johnson D, Frexes-Steed M, et al. A pilot study of neoadjuvant paclitaxel and radiation with correlative molecular studies in stage II/III breast cancer. Clin Breast Cancer. 2000; 1(1):68–71. [PubMed: 11899393]
31. Ikui AE, Yang CP, Matsumoto T, Horwitz SB. Low concentrations of taxol cause mitotic delay followed by premature dissociation of p55CDC from Mad2 and BubR1 and abrogation of the spindle checkpoint, leading to aneuploidy. Cell Cycle. 2005; 4(10):1385–8. [PubMed: 16138009]
32. Martinez-Exposito MJ, Kaplan KB, Copeland J, Sorger PK. Retention of the BUB3 checkpoint protein on lagging chromosomes. Proc Natl Acad Sci U S A. 1999; 96(15):8493–8. [PubMed: 10411903]
33. Alexander S, Koehl GE, Hirschberg M, Geissler EK, Friedl P. Dynamic imaging of cancer growth and invasion: a modified skin-fold chamber model. Histochem Cell Biol. 2008; 130(6):1147–54. [PubMed: 18987875]
34. Wang X, Zhao G, Van S, Jiang N, Yu L, Vera D, et al. Pharmacokinetics and tissue distribution of PGG-paclitaxel, a novel macromolecular formulation of paclitaxel, in nu/nu mice bearing NCI-460 lung cancer xenografts. Cancer Chemother Pharmacol. 2010; 65(3):515–26. [PubMed: 19593566]

35. Mason KA, Milas L, Peters LJ. Effect of paclitaxel (taxol) alone and in combination with radiation on the gastrointestinal mucosa. Int J Radiat Oncol Biol Phys. 1995; 32(5):1381–9. [PubMed: 7635778]

36. Schiemann K, Finsinger D, Zenke F, Amendt C, Knochel T, Bruge D, et al. The discovery and optimization of hexahydro-2H-pyrano[3,2-c]quinolines (HHPQs) as potent and selective inhibitors of the mitotic kinesin-5. Bioorg Med Chem Lett. 2010; 20(5):1491–5. [PubMed: 20149654]

37. Shi J, Orth JD, Mitchison T. Cell type variation in responses to antimitotic drugs that target microtubules and kinesin-5. Cancer Res. 2008; 68(9):3269–76. [PubMed: 18451153]

38. Symmans FW. Breast cancer response to paclitaxel in vivo. Drug Resist Updat. 2001; 4(5):297–302. [PubMed: 11991683]

39. Huang HC, Shi J, Orth JD, Mitchison TJ. Evidence that mitotic exit is a better cancer therapeutic target than spindle assembly. Cancer Cell. 2009; 16(4):347–58. [PubMed: 19800579]

40. Yang R, Niepel M, Mitchison TJ, Sorger PK. Dissecting variability in responses to cancer chemotherapy through systems pharmacology. Clin Pharmacol Ther. 2010; 88(1):34–8. [PubMed: 20520606]

41. Zhou F, Xing D, Wu S, Chen WR. Intravital imaging of tumor apoptosis with FRET probes during tumor therapy. Mol Imaging Biol. 2009; 12(1):63–70. [PubMed: 19543775]

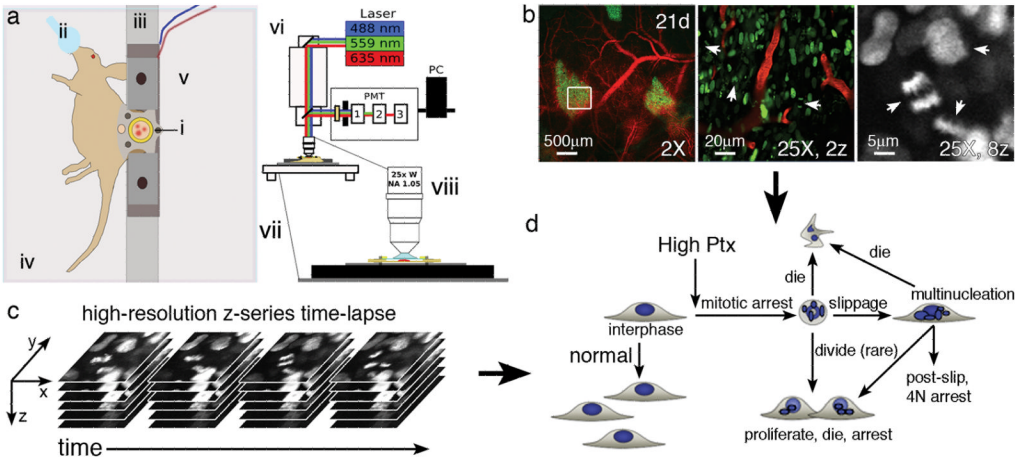

Figure 1.

In vivo pharmacodynamic microscopy (IPDM). a) The imaging system. Xenograft tumor(s) in the DSC (i); anesthesia (ii); temperature-regulated holding bar (iii); temperature-regulated stage (iv); DSC holding plate and finger screws (v); laser scanning confocal microscope (vi); charged-air table (vii); objective (viii). PC, personal computer. b) HT-1080 tumor expressing H2b-EGFP (green) with Angiosense-680 labeled blood vessels (red). Microscopy at different resolutions allows for the identification of mitotic profiles (arrows) and specific mitotic stages (arrows). 2z; 25X lens, 2X zoom. 8z; 25X lens, 8X zoom. c) Z-series time-lapse microscopy. d) In culture, the Ptx response shows high intra-cell line variability. After mitotic arrest cells can progress along multiple pathways. Z-series imaging (b) and z-series time-lapse (c) were used to study mitosis and Ptx-response.

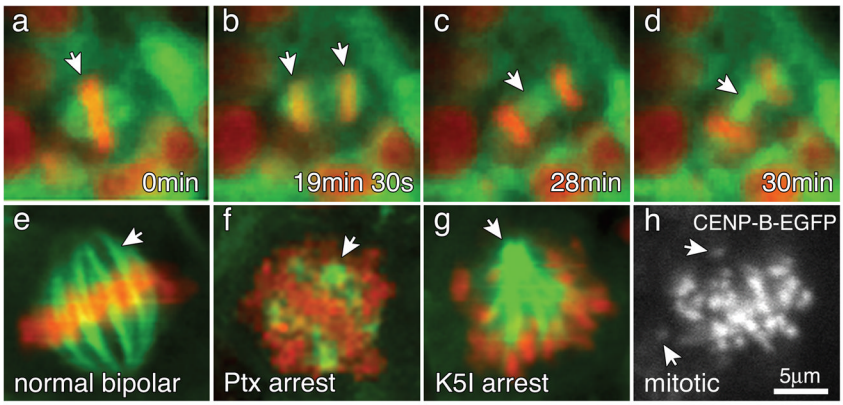

Figure 2.

Mitosis and mitotic spindle structures via IPDM. a–d) HeLa H2b-mCherry/tubulin-EGFP cells. All stages of mitosis can be observed. See supplemental movie 1. Arrows (a, b); chromosomes. Arrows (c, d); microtubule mid-zone. e) Normal mitotic cell at higher magnification reveals kinetochore fibers (arrow). f, g) Different anti-mitotic drug-induced phenotypes. f) Ptx-arrested mitotic cell showing microtubule rosettes surrounded by chromosomes (arrow). g) K5I-arrested mitotic cell showing monopolar spindle (arrow) surrounded by chromosomes. h) Mitotic U2 OS cell expressing CENP-B-EGFP (kinetochore). Kinetochores spots ≤500nm were resolved. (ad) acquired at 20X, (e–h) acquired at 20X, 8.5X zoom. Scale bar (h) applies to all images.

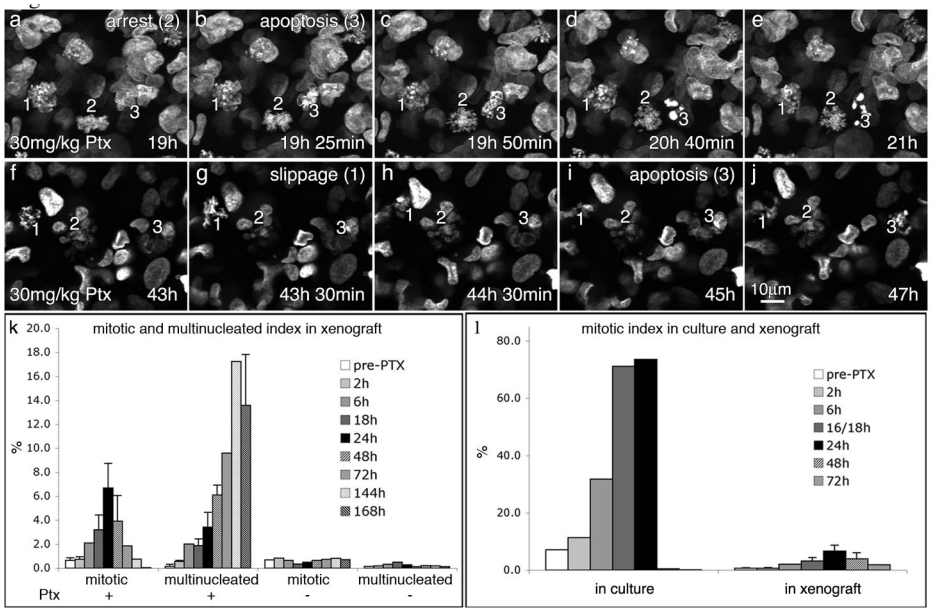

Figure 3.

Time-lapse microscopy and analysis of mitotic events following saturating Ptx. 30mg/kg Ptx was used. a–e) 19h post-Ptx cells. See supplemental movie 3. a) Cell 1 is arrested, cell 2 is early arrest, cell 3 is post-slippage. b) 25min later cell 3 died. c–e) Cells 1 and 2 remained arrested. The DNA in cell 3 becomes condensed. f–j) Same tumor, 43h post-Ptx. See supplemental movie 4. f) Cell 1 is arrested, cells 2 and 3 are multinucleated. g–j) 30min later, cell 1 slipped from arrest and persisted. f–j) Cell 2 remained multinucleated. Cell 3 died at ~45h post-Ptx. k) In vivo analysis of mitotic and multinucleated index. The peak mitotic index was ~7% at 24h and decreased to below pre-Ptx levels by 168h. The multinucleated index increased subsequent to mitotic index and remained elevated. l) Comparison of indices in culture and in vivo. The pre-Ptx mitotic index in culture is higher than the xenograft and peaked at ~75% at 24h after Ptx, compared to ~7% at 24h in the xenograft. In culture 240 cells were tracked. In vivo, over 1000 cells were scored for each time-point. Time-lapses acquired at 25X, 1.5X zoom. Scale bar (j) applies to all images.

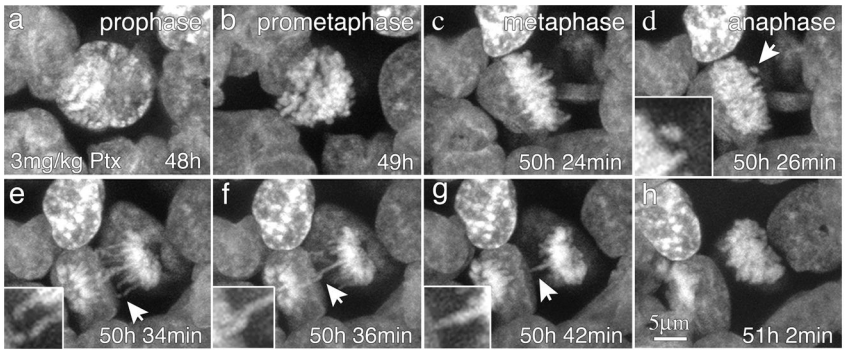

Figure 4.

Low-dose Ptx results in mitotic delay and chromosome missegregation. 48 hours after 3mg/kg Ptx, a cell in prophase was imaged at 2min intervals using a 60X, NA 1.10 water immersion lens. See supplemental movie 6. a–c) This cell required 2h 24min to reach metaphase; the last frame before anaphase. d) Upon anaphase, a single chromosome or chromosome pair progressed pole-ward separately from the others (arrow, inset). e–g) Additional chromosomes were stretched during anaphase. h) This cell required ≥3h to complete mitosis, 2-fold longer than normal. Scale bar (h) applies to all images.

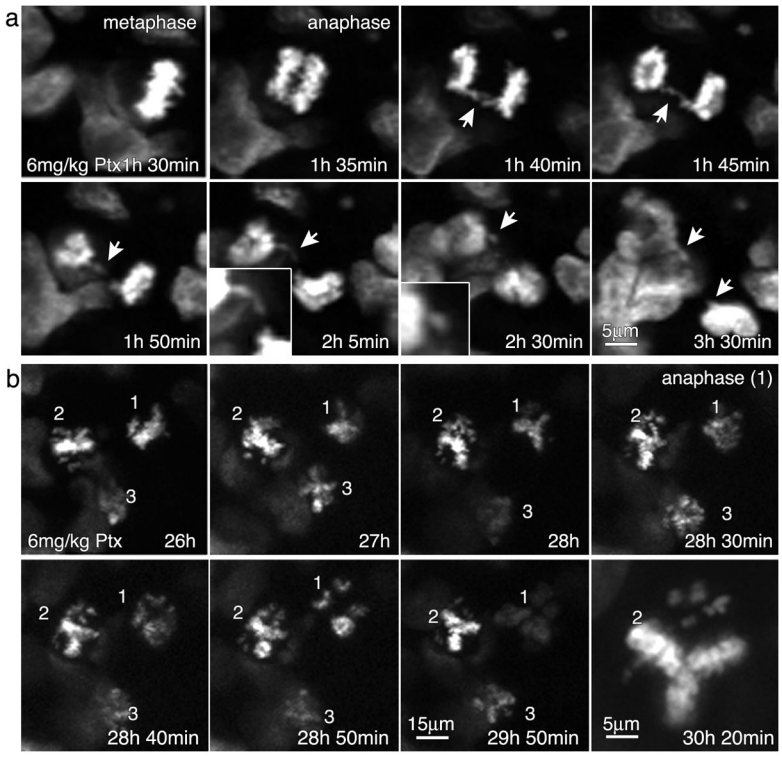

Figure 5.

In vivo time-lapse reveals PD principles of Ptx. 6mg/kg Ptx was used. a) After 1h 30min Ptx, a late prometaphase cell was imaged. This cell enters anaphase and initially appeared normal. Lagging chromosomes (arrows, inset) were present that subsequently resulted in micronuclei formation (arrows, insets, supplemental movie 7). b) Multipolar mitosis occurs after 6mg/kg Ptx. At 26h Ptx, time-lapse of random areas was performed. See supplemental movie 8. Three cells (1, 2, 3) are initially mitotic. By 28h, cell 1 is multipolar while cells 2 and 3 are arrested. Cell 1 underwent multipolar anaphase, cell 2 progressed toward a multipolar alignment and cell 3 remained arrested. High-magnification of cell 2 at 30h 20 min Ptx shows unaligned chromosomes. Note: it required >4h for cell 2 to become multipolar, indicating mitotic progression is delayed. Time-lapses acquired at 25X, 1.5X zoom.

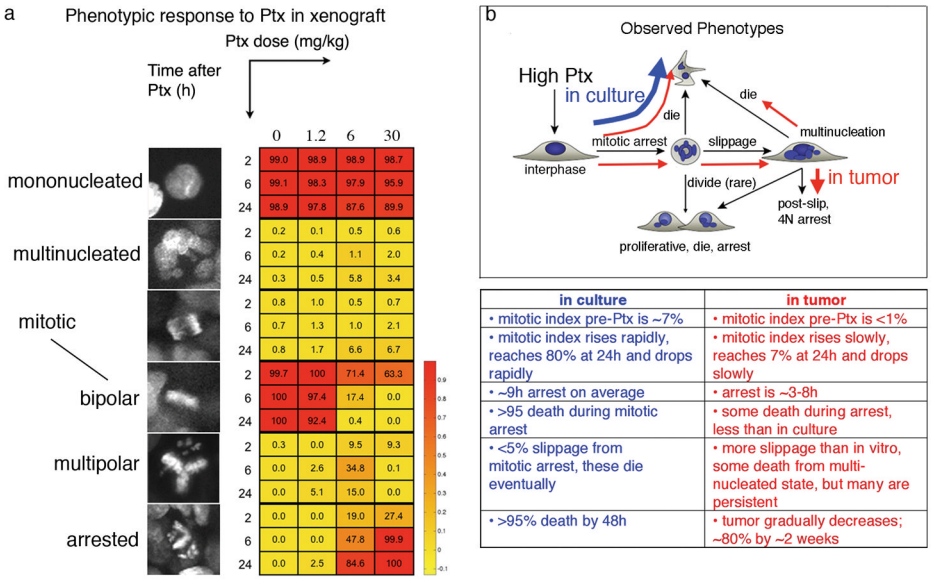

in culture	in tumor
• mitotic index pre-Ptx is ~7%	• mitotic index pre-Ptx is <1%
• mitotic index rises rapidly, reaches 80% at 24h and drops rapidly	• mitotic index rises slowly, reaches 7% at 24h and drops slowly
• ~9h arrest on average	• arrest is ~3-8h
• >95 death during mitotic arrest	• some death during arrest, less than in culture
• <5% slippage from mitotic arrest, these die eventually	• more slippage than in vitro, some death from multi-nucleated state, but many are persistent
• >95% death by 48h	• tumor gradually decreases; ~80% by ~2 weeks

Figure 6.

IPDM can be used to establish Ptx-PD over time and dose and Ptx response is significantly different in vivo than in culture. a) Phenotypic responses are color coded in response to increasing doses of Ptx at 2, 6 and 24h treatment. The majority of cells remained mononucleated during the first 24h and both 6 and 30mg/kg showed increasing multinucleated and mitotic indices. In order to establish PD of Ptx on mitosis, mitotic profiles were further separated to include bipolar, multipolar and arrested phenotypes. As the percent of bipolar cells decreases the multipolar and arrested phenotypes increase. For 1.2mg/kg Ptx a small increase in multipolarity and arrest occurred at 24h. For 6mg/kg, by 6h >30% were multipolar, which remained at 15% at 24h; the percent of arrested cells steadily increased to 24h. Unlike 1.2 and 6mg/kg, 30mg/kg did not accumulate or maintain significant multipolarity. After 2h, the percent multipolar sharply decreased and all mitotics displayed an arrested phenotype. b) Summary of in culture and in tumor response to saturating Ptx.